Impact of molecular architecture and adsorption density on adhesion of mussel-inspired surface primers with catechol-cation synergy

George D. Degen,¹ Parker R. Stow,² Robert B. Lewis,² Roberto C. Andresen Eguiluz,¹ Eric Valois,³ Kai Kristiansen,¹ Alison Butler,^{2*} Jacob N. Israelachvili^{1,4}

¹Department of Chemical Engineering, ²Department of Chemistry and Biochemistry, ³Biomolecular Science and Engineering, and ⁴Materials Department, University of California, Santa Barbara, California 93106, United States

ABSTRACT: Marine mussels secrete proteins rich in residues containing catechols and cationic amines that displace hydration layers and adhere to charged surfaces under water via a cooperative binding effect known as catechol-cation synergy. Mussel-inspired adhesives containing paired catechol and cationic functionalities are a promising class of materials for biomedical applications, but few studies address the molecular adhesion mechanism(s) of these materials. To determine whether intramolecular adjacency of these functionalities is necessary for robust adhesion, a suite of siderophore analog surface primers was synthesized with systematic variations in intramolecular spacing between catechol and cationic functionalities. Adhesion measurements conducted with a surface forces apparatus (SFA) allow adhesive failure to be distinguished from cohesive failure and show that the failure mode depends critically on the siderophore analog adsorption density. The adhesion of these molecules to muscovite mica in an aqueous electrolyte solution demonstrates that direct intramolecular adjacency of catechol and cationic functionalities is not necessary for synergistic binding. However, we show that increasing the catechol-cation spacing by incorporating non-binding domains results in decreased adhesion, which we attribute to a decrease in the density of catechol functionalities. A mechanism for catechol-cation synergy is proposed based on electrostatically driven adsorption and subsequent binding of catechol functionalities. This work should guide the design of new adhesives for binding to charged surfaces in saline environments.

1. INTRODUCTION

Rational design of wet adhesives requires an understanding of the intermolecular interactions between adhesives and substrates in saline environments such as seawater or body fluids. Designing adhesives for use in these environments is challenging—for example, van der Waals forces are significantly reduced under water, and ions in solution compete with adhesives for binding sites on charged surfaces. Despite these challenges, marine mussels adhere to many inorganic and organic surfaces, 1-3 typically by relying on adhesive proteins rich in the catecholic amino acid 3,4-dihydroxyphenylalanine (Dopa).4 Due to the large proportion of cationic residues, most commonly lysine, paired with Dopa in the most adhesive interfacial mussel protein (Mfp-5), 1,5 it has been hypothesized that both these residues are important for adhesion. Furthermore, other compounds containing catechol and cationic functionalities have been shown to adhere to many surfaces. Polydopamine, formed from the polymerization and self-assembly of oxidized dopamine, 6-9 adheres to a wide variety of materials and has been proposed for many applications.¹⁰ Other adhesives containing catechol and cationic functionalities include catechol-chitosan¹¹⁻¹³ and catechol-poly(ethylenimine),^{14,15}

among others.^{16,17} Molecules containing Dopa and other catechols adhere to apatite¹⁸ and metal oxide¹⁹ surfaces found in bone and implant materials, and have been shown to be biocompatible,²⁰ making them attractive alternatives to existing medical adhesives, many of which are ineffective^{21,22} or cytotoxic.^{23–25}

Despite widespread scientific and applications-based research on materials containing catechol functionalities,20 specific adhesion mechanisms of these materials have only recently begun to be explored.²⁶ It has been demonstrated that adhesives incorporating catechol and cationic amine functionalities bind more strongly to muscovite mica in saline solutions than adhesives incorporating either catechols or cations alone, 27 a cooperative effect known as catecholcation synergy. The adjacent pairing of Dopa and lysine in the Mfp-5 sequence⁵ has prompted speculation that intramolecular proximity of catechol and cationic functionalities may be necessary for adhesion, and that an intramolecular cut-off distance may exist beyond which catechol-cation synergy no longer operates.²⁸ A recent study showed that the order of catechol and cationic functionalities impacts the single-molecule pull-off force,29 supporting the hypothesis that direct adjacency of catechol and cationic functionalities may be enhance adhesion. However, until now no study has directly explored the impact of intramolecular spacing on catechol-cation synergy.

Here, we present adhesion measurements of films of siderophore analog surface primers with systematically varying intramolecular spacing between catechol and cationic amine functionalities. We show that the pull-off force mediated by the siderophore analogs depends critically on the adsorption density and confirm that catechol-cation synergy enables adhesion. Surprisingly, the results demonstrate that direct intramolecular adjacency between catechol and cationic functionalities is not necessary for catechol-cation synergy and suggest that no intramolecular cutoff distance between these functionalities exists for which catechol-cation synergy will be abolished. To explain the results, we propose a mechanism for catechol-cation synergy based on electrostatically driven adsorption and support this mechanism with a qualitative model.

2. EXPERIMENTAL SECTION

We synthesized a suite of seven siderophore analogs, synthetic mimics of bacterial iron chelators called siderophores.30 Each analog has a central tris(2-aminoethyl)amine (Tren) scaffold with three identical peptide arms. Here, each peptide arm contained glycine and lysine and were capped with either the catechol 2,3-dihydroxybenzoyl (2,3-DHBA) or benzoyl functionality (Figure 1). The intramolecular spacing between 2,3-DHBA and lysine in the peptide arms was varied by changing the peptide sequence. Three of the analogs were isomers: Tren(GGK-Cat)₃, Tren(GKG-Cat)₃, and Tren(KGG-Cat)₃. Tren denotes the tris(2-aminoethyl)amine scaffold, G and K denote glycine and lysine, respectively, and Cat denotes 2,3-DHBA. Siderophore analogs with even greater catechol-cation spacing (Tren(KGGG-Cat)3 and Tren(KGGGGGG-Cat)3), cationic amines but without catechols (Tren(GGK-Benz)₃), and only catechols (Tren(GGG-Cat)₃) were also synthesized. Additional details on materials, synthesis, and molecular characterization are included in the Supporting Information (S1 and S2). Analogs were dissolved at 1 mM in an aqueous salt solution (50 mM acetic acid, 150 mM KNO₃, pH = 3.3), chosen to mimic physiological ionic strengths but avoid catechol oxidation by maintaining an acidic pH.

Adhesion measurements were performed using a surface forces apparatus (SFA) model SFA2000 (SurForce, LLC), described in detail in the Supporting Information (S3) and elsewhere.31 In the SFA, freshly cleaved muscovite mica surfaces were arranged in a crossed cylinder geometry. All experiments were performed at a constant temperature. Siderophore analogs were deposited via adsorption from solution into films on either one (asymmetric deposition) or both (symmetric deposition) mica surfaces. For asymmetric deposition, 50 µL of 400 µM siderophore analog solution was injected onto one of the mica surfaces and incubated for at least 60 min. The surface was then rinsed before adhesion measurements. For symmetric deposition, siderophore analog solution was injected into a capillary meniscus between both surfaces (final concentration 90-667 μ M). The surfaces were incubated for at least 60 min and were not rinsed before adhesion measurements.

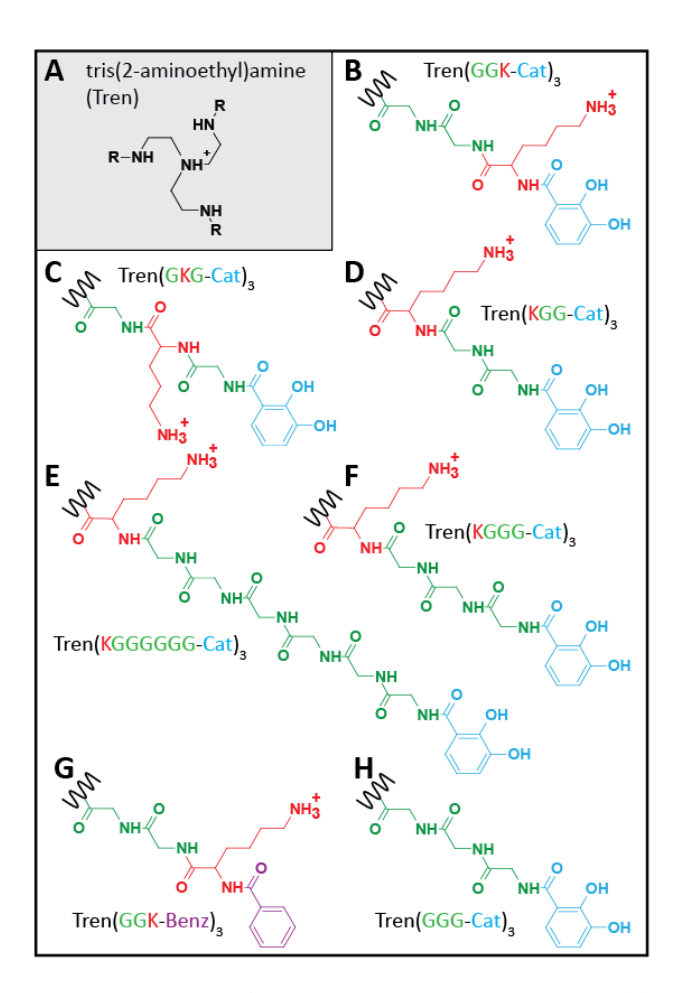


Figure 1. The suite of siderophore analogs investigated. (A) Tris(2-aminoethyl)amine (Tren) scaffold. R-groups are shown in (B)-(H). The intramolecular distance between 2,3-DHBA and lysine is varied in (B) Tren(GGK-Cat)₃, (C) Tren(GKG-Cat)₃, (D) Tren(KGG-Cat)₃, (E) Tren(KGGGGGG-Cat)₃, and (F) Tren(KGGG-Cat)₃. Analogs containing lysine without 2,3-DHBA, (G) Tren(GGK-Benz)₃, and 2,3-DHBA without lysine, (H) Tren(GGG-Cat)₃ were also synthesized.

Adhesion measurements were performed with the mica surfaces bridged by a capillary meniscus of ~50 μL salt solution (50 mM acetic acid, 150 mM KNO₃, pH = 3.3) at a constant temperature ($T = 22 \pm 1$ °C). Normal force (F) and surface separation distance (D) were measured during cycles of i) approach and compression, ii) waiting at maximum compression (t_{wait}), and iii) separation and jump from contact were performed at constant approach and separation velocities. Measured forces were normalized by the average radius of curvature of the surfaces (R). Pull-off force $(-F_{ad}/R)$ was calculated from the distance that the surfaces jumped from contact during separation corresponding to the most negative force measured during separation. Pull-off force did not depend on separation velocity ($V_{\text{out}} = 2-10 \text{ nm/s}$) (Figure S32) nor maximum compression (F/R = 9-108mN/m). We use the term "pull-off" instead of "adhesion" because the force required to separate the mica surfaces can correspond to adhesive failure at the film-mica interface, cohesive failure at the film-film interface, or a combination of the two failure modes. The separation distance during compression of the surfaces at which the force exceeded 1 mN/m was denoted the onset of interaction (D_{onset}). The surface separation distance measured at maximum compression was denoted compressed film thickness (Dt). The change in film thickness after waiting at maximum compression (ΔD_t) was reported as the difference between compressed film thicknesses measured before and after waiting at maximum compression. Error bars correspond to the standard deviation, with an additional contribution to the error in D_t for 6 of the data points from measuring D_t relative to the D_t measured in salt solution. To characterize film coverage, atomic force microscopy (AFM) imaging was performed on mica immersed in salt solution (50 mM acetic acid, 150 mM KNO₃, pH = 3.3) with an MFP-3D Bio AFM (Asylum Research, Goleta, CA), described in the Supporting Information (S4).

3. RESULTS AND DISCUSSION

We used a surface forces apparatus (SFA) to directly test whether intramolecular proximity is necessary for catechol-cation synergy by measuring the adhesion to mica of siderophore analogs with systematically varying spacing between catechol and cationic amine functionalities. In adhesion measurements, two failure modes can contribute to the measured pull-off force: adhesive failure (separation at the film-mica interface) and cohesive failure (separation at the film-film interface). When adhesive failure occurs, the pull-off force corresponds to intermolecular interactions between siderophore analogs and mica, which can include bidentate hydrogen bonds and coordinate covalent bonds.4 When cohesive failure occurs, the pull-off force corresponds to intermolecular interaction between siderophore analogs adsorbed on each mica surface, which can include hydrogen bonds, hydrophobic interactions, and cation-pi interactions.4 Catechol-cation synergy refers to cooperative binding of molecules to a substrate. Therefore, to assess the impact of molecular structure on catechol-cation synergy, it is necessary to measure pull-off forces corresponding to adhesive failure. For the case of molecularly smooth mica surfaces (Figure S41), a monolayer film between the surfaces guarantees adhesive failure because each siderophore analog within the monolayer can bind to both mica surfaces, and therefore separation must occur at the film-mica interface. Below, we establish the deposition conditions resulting in a monolayer of siderophore analogs between the surfaces, and therefore adhesive failure. We then confirm that catechol-cation synergy occurs and discuss the impact of intramolecular catechol-cation spacing on the synergy.

Compression and separation of films of siderophore analogs in an SFA enabled measurement of pull-off force $(F_{\rm ad}/R)$, onset of interaction $(D_{\rm onset})$, and compressed film thickness $(D_{\rm t})$. Figure 2 shows representative plots of normal force (F/R) vs. surface separation distance (D) measured for films of Tren(GGK-Cat)₃, Tren(GKG-Cat)₃, and Tren(KGG-Cat)₃. Each plot corresponds to an experiment conducted using a single pair of mica surfaces. First, bare mica surfaces were compressed and separated in salt solution (black circles). Next, a film of siderophore analogs was deposited onto one of the mica surfaces via asymmetric deposition, followed by compression and separation of the surfaces (red circles). Finally, analogs were deposited

symmetrically onto both surfaces, and the surfaces were again compressed and separated (blue circles). Open circles correspond to approach and compression of the surfaces; closed circles correspond to separation and jump from contact. In each plot, $F_{\rm ad}/R$, $D_{\rm t}$, and $D_{\rm onset}$ are indicated.

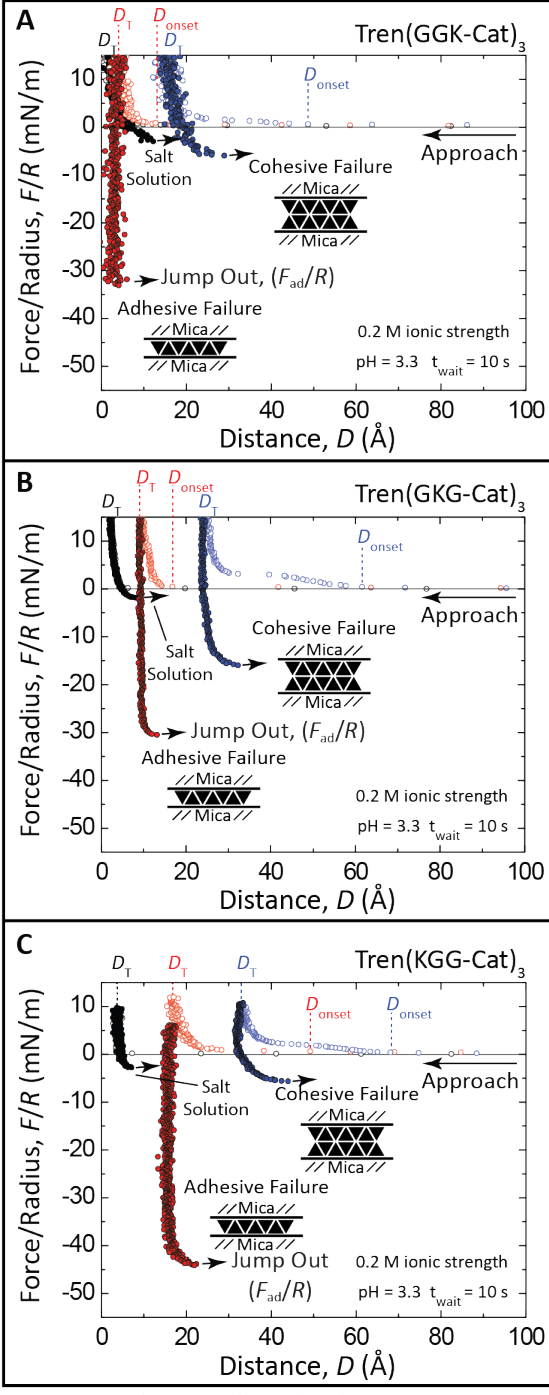


Figure 2. Plots of normal force (F/R) vs. separation distance (D) for bare mica surfaces (black circles) and after asymmetric (red circles) and symmetric (blue circles) depositions of (A) Tren(GGK-Cat)₃, (B) Tren(GKG-Cat)₃, and (C) Tren(KGG-Cat)₃. Open circles show approach and compression of the surfaces; closed circles show separation and jump from contact.

Pull-off force, onset of interaction, and contact time dependence measured during compression and separation of films of siderophore analogs depended on the compressed film thickness. Figure 3 shows plots of pull-off force (- $F_{\rm ad}/R$) as a function of compressed film thickness (D_t). For each analog, $D_t < 10$ Å corresponds to low pull-off force. Pull-off force is maximized at $D_t = 10$ Å, and the maximum pull-off forces mediated by each analog are not statistically significantly different ($\alpha = .05$) (Figure S33). As D_t increases 10 Å, pull-off force decreases. Interestingly, the analog with the greatest separation between catechol and cationic functionalities (Tren(KGG-Cat)₃) mediates larger pull-off forces than Tren(GKG-Cat)₃ and Tren(GGK-Cat)₃ for 15 Å < D_t < 20 Å, discussed later.

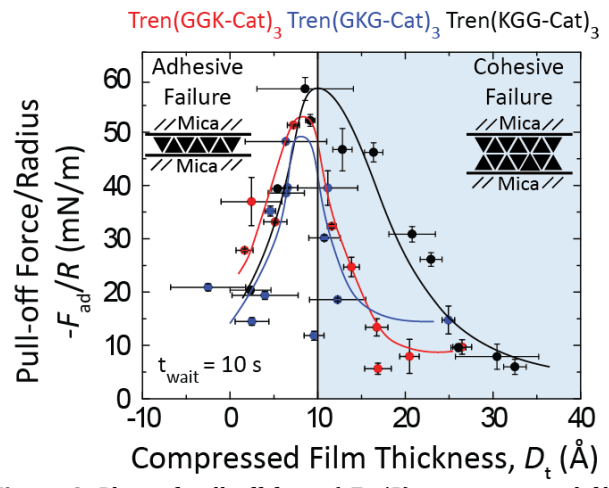


Figure 3. Plots of pull-off force $(-F_{ad}/R)$ vs. compressed film thickness (D_t) for Tren(GGK-Cat)₃ (red circles), Tren(GKG-Cat)₃ (blue circles), and Tren(KGG-Cat)₃ (black circles). Lines are included to guide the eye.

The compressed film thickness corresponding to maximum pull-off force ($D_t = 10 \text{ Å}$) also corresponds to a discontinuous increase in the onset of interaction (D_{onset}). Figure 4 shows plots of D_{onset} as a function of D_{t} . As D_{t} increases from 0 to 10 Å, D_{onset} increases from 5 to 15 Å. At $D_{\text{t}} = 10$ Å, D_{onset} increases discontinuously from 15 to 40 Å. As Dt increases further from 10 to 30 Å, Donset increases from 40 to 60 Å. Dt = 10 Å also corresponds to a minimum increase in pull-off force with increased contact time. Figure 5A shows pull-off force for $t_{\text{wait}} = 60 \text{ min } (F_{t = 60 \text{ min}})$, normalized by pull-off force for $t_{\text{wait}} = 10 \text{ s}$ ($F_{t=10 \text{ s}}$), as a function of D_{t} . For all analogs, increased contact time generally results in increased pull-off force ($F_{\rm t=60\,min}/F_{\rm t=60\,min} \ge 1$). However, the increase in pull-off force is minimized for $D_t = 10 \text{ Å}$ ($F_{t=60 \text{ min}}/F_{t=10 \text{ s}} =$ 1.0). Increased contact time also decreases D_t . Figure 5B shows the change in compressed film thickness ΔD_t as a function of Dt measured before the wait time. Open circles correspond to short waiting times ($t_{\text{wait}} = 10 \text{ s}$) for which D_{t} did not decrease ($\Delta D_t = 0$). In contrast, closed circles correspond to longer contact times ($t_{\text{wait}} = 60 \text{ min}$) and decreases in D_t ($\Delta D_t > 0$), with the largest decreases occurring for $D_t > 0$ 10 Å.

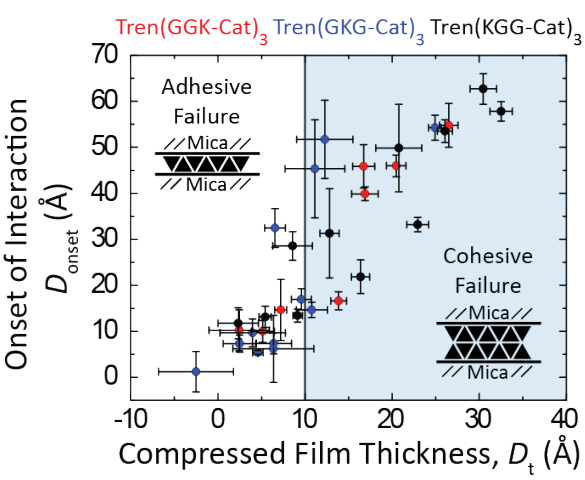


Figure 4. Plots of onset of interaction (D_{onset}) vs. compressed film thickness (D_t) for Tren(GGK-Cat)₃ (red circles), Tren(GKG-Cat)₃ (blue circles), and Tren(KGG-Cat)₃ (black circles).

As shown above, the maximum pull-off force, discontinuous increase in the onset of interaction, and minimum increase in pull-off force with waiting time all occur for the same compressed film thickness ($D_t = 10 \text{ Å}$). Taken together, the relationships between these quantities suggest that this film thickness corresponds to a monolayer of siderophore analogs between the surfaces. For $D_t > 10 \text{ Å}$, a transition occurs from a single monolayer between the mica surfaces to two monolayers, one on each mica surface. This transition results in a corresponding transition from adhesive failure to cohesive failure. For reference, Figure 6 shows a schematic diagram of mica surfaces before and after asymmetric or symmetric deposition of siderophore analogs at different surface densities. Panels i. and iv. show mica surfaces prior to deposition of siderophore analogs. Panels ii., iii, v. and vi. show single monolayers between the surfaces and adhesive failure. Panel vii. shows a monolayer on each surface and cohesive failure. Below, we relate our results to a transition from adhesive failure to cohesive failure and interpret measured pull-off forces in the context of catechol-cation synergy.

We attribute the low pull-of force and onset of interaction for D_t < 10 Å to a sparse monolayer between the mica surfaces. A sparse monolayer contains relatively few siderophore analog molecules binding to both surfaces, and therefore is expected to mediate a low pull-off force, consistent with the data shown in Figure 3. A sparse monolayer between the surfaces can be established by either asymmetric deposition (Figure 6 ii.) or symmetric deposition (Figure 6 v.) with a low concentration of siderophore analogs in solution. We note that waiting at maximum compression results in disproportionate increases in the pull-off force mediated by Tren(GKG-Cat)₃ relative to the other analogs for $D_t < 10$ Å (Figure 5A, blue circles). Separation of the glycine residues in Tren(GKG-Cat)3 may reduce the conformational flexibility and inhibit initial binding to both mica surfaces. Time in contact may enable rearrangement and binding to both mica surfaces of individual Tren(GKG-Cat)₃ molecules, thus increasing the pull-off force.

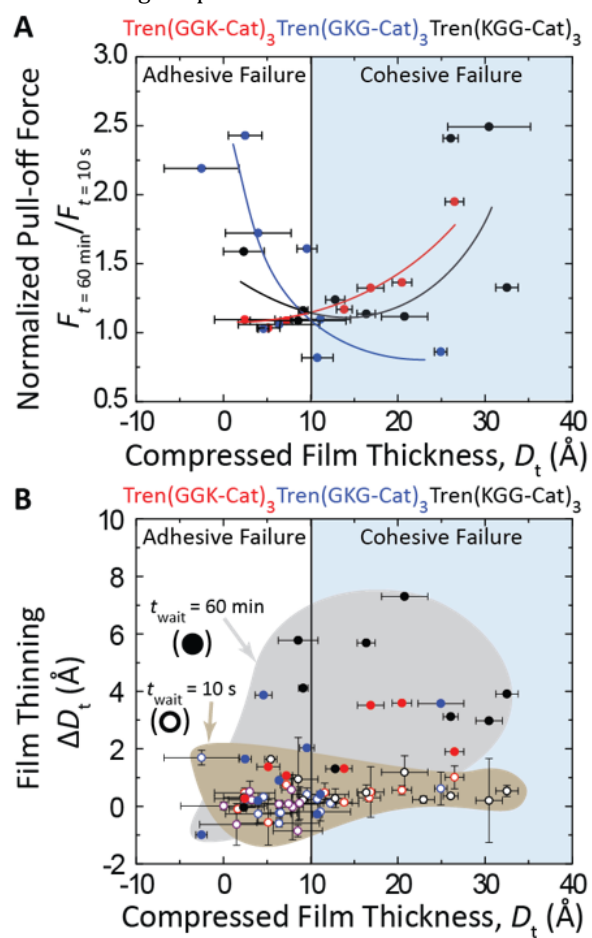


Figure 5. (A) Plots of normalized pull-off force $(F_{t=60 \text{ min}}/F_{t=10 \text{ s}})$ vs. compressed film thickness (D_t) for Tren(GGK-Cat)₃ (red circles), Tren(GKG-Cat)₃ (blue circles), and Tren(KGG-Cat)₃ (black circles). Lines are included to guide the eye. (B) Corresponding plots of change in film thickness (ΔD_t) vs. D_t for $t_{\text{wait}} = 10 \text{ s}$ (open circles) and $t_{\text{wait}} = 60 \text{ min}$ (closed circles).

The maximum pull-off force and minimum increase in pull-off force with waiting time occur for $D_t = 10 \text{ Å}$, suggesting that this film thickness corresponds to a single densely packed monolayer between the surfaces. The ability of siderophore analogs to form films of varying density was confirmed with AFM imaging—increasing the concentration of siderophore analogs in solution during incubation increases the density of the film on the mica surface (Figure S31). Like a sparse monolayer, a densely packed monolayer can result from asymmetric deposition of siderophore analogs onto one of the surfaces (Figure 6 iii.), or from symmetric deposition of a sparse monolayer of analogs onto both surfaces (Figure 6 vi.). When these sparse monolayers are brought into contact, they combine to form a densely packed monolayer. Regardless of the deposition method, a densely packed monolayer is expected to maximize the number of siderophore analogs binding to both mica surfaces and therefore maximize the pull-off force, consistent with the data shown in Figure 3. The minimum increase in pull-off force with waiting time also occurs at $D_t = 10 \text{ Å}$,

providing additional evidence that this compressed film thickness corresponds to a densely packed monolayer. Dense packing of analogs on a surface and a corresponding low surface area per molecule may prevent functional groups in each molecule from binding to the surface, leaving the groups free to bind to the adjacent surface upon contact. Therefore, increased contact time does not change the distribution of functionalities binding to each surface and pull-off force remains constant.

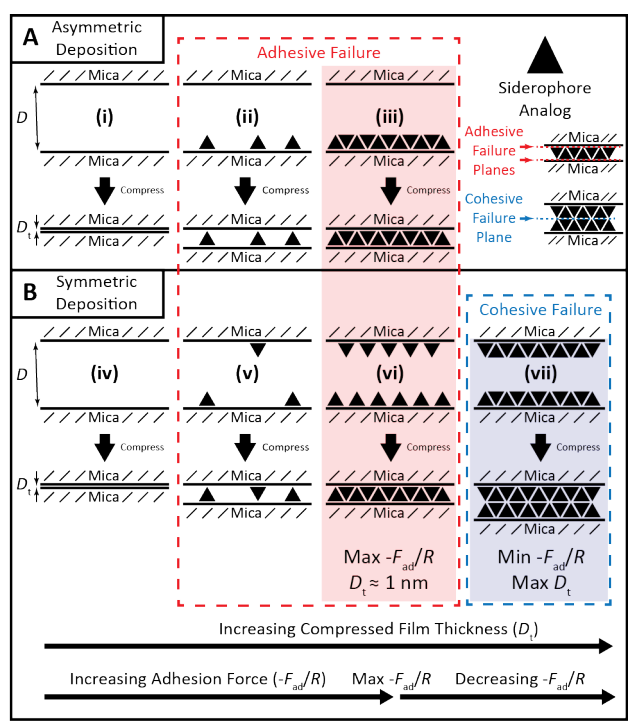


Figure 6. A transition from one monolayer (adhesive failure) to two monolayers (cohesive failure) decreases pull-off force ($F_{\rm ad}/R$) and increases compressed film thickness ($D_{\rm t}$). (A) Asymmetric deposition of siderophore analogs on a single surface yields adhesive failure, shown in (ii) and (iii). (B) Symmetric deposition of siderophore analogs on both surfaces results in either adhesive failure shown in (v) and (vi) or cohesive failure shown in (vii). (ii) and (v) show configurations with the same pull-off force; configurations with maximum pull-off force are shown in (iii) and (vi). Bare mica surfaces before deposition of siderophore analogs are shown in (i) and (iv).

The discontinuous increase in onset of interaction for Dt > 10 Å indicates a transition from a single densely packed monolayer to two monolayers between the surfaces. With a monolayer on each surface, repulsive forces begin when the films on each surface contact each other. This distance (D_{on} set = 40 Å) is slightly more than double the onset of interaction for a single densely packed monolayer ($D_{onset} = 15 \text{ Å}$), consistent with a transition from one to two monolayers. The largest compressed film thickness ($D_t = 30 \text{ Å}$) corresponds to D_{onset} = 60 Å. This value is larger than would be expected for symmetric densely packed monolayers, suggesting that additional siderophore analogs can adsorb onto the monolayers on each surface. However, no evidence of an adsorbed layer beyond a monolayer is seen after asymmetric deposition, suggesting that the siderophore analogs loosely adsorb to the monolayer and are removed during the rinsing associated with asymmetric deposition. We note that D_t is not expected to increase discontinuously during a transition from one to two monolayers because D_t depends on the adsorption density of the monolayers. A densely packed monolayer is expected to have a larger D_t than a sparse monolayer because individual molecules occupy less area on the surface and therefore extend further into solution. Similar behavior is also seen in adsorbed surfactant monolayers. As a result, the discontinuous increase in D_{onset} reveals the transition from one to two monolayers in a way that D_t does not.

The decreasing pull-off force with increasing film thickness for $D_t > 10$ Å provides additional evidence of a transition from a single densely packed monolayer to two monolayers between the surfaces by indicating a transition from adhesive failure to cohesive failure. An adhesive system is expected to fail at the weakest interface. If the film-film interface were stronger than the film-mica interface, adhesive failure would continue to occur at the film-mica interface, regardless of the value of Dt. In that case, pull-off force would not decrease with increasing D_t . Here, the pull-off force decreases with increasing D_{t} , suggesting a transition from adhesive to cohesive failure. We propose that as the monolayers on each surface become more densely packed, peptide arms on siderophore analogs in each monolayer become unable to penetrate the adjacent monolayer and therefore fail to bind to both mica surfaces. Instead, pull-off forces correspond to cohesive failure and interactions between analogs in opposite films (Figure 6 vii.). The decrease in molecular interdigitation with increasing film density is analogous to the behavior of polymer brushes used for antibiofouling surfaces: increasing polymer grafting density decreases the ability of small peptide adhesives to penetrate the brush layer and bind to the underlying substrate.33 Consistent with this interpretation, the highest incubation concentration of siderophore analogs during symmetric deposition resulted in the lowest pull-off forces (Figure S31). We note that when a bare mica surface is brought into contact with a monolayer of siderophore analogs on the opposite surface (as occurs after asymmetric deposition), siderophore analogs may transfer from one surface to the other upon separation of the surfaces, ultimately resulting in the same distribution of siderophore analogs on each surface as the symmetric deposition configuration shown in Figure 6 vi.

The increase in pull-off force and decrease in film thickness with waiting time for $D_t > 10$ Å suggest a partial transition from cohesive failure to adhesive failure. We attribute this transition to interdigitation of siderophore analogs in monolayers on each surface. Here, interdigitation refers to peptide arms of the siderophore analogs penetrating the opposite film and binding to the underlying mica surface. Increasing the fraction of individual siderophore analogs binding to both mica surfaces results in an increased ratio of adhesive failure to cohesive failure, and consequently an increased pull-off force. Interdigitation likely also results in partial coalescence of the two films, consistent with the decrease in film thickness ($\Delta D_t > 0$) after increased waiting time reported in Figure 5B for $D_t > 10$ Å.

As stated above, Tren(KGG-Cat)3, mediated larger pull-off forces than Tren(GKG-Cat)₃ and Tren(GGK-Cat)₃ for 15 Å < $D_{\rm t}$ < 20 Å (Figure 3). The increased pull-off force at these film thicknesses suggests that the glycine residues in Tren(KGG-Cat)₃ give the catechols independent mobility from the surface-bound lysines,34 enabling them to penetrate the film on the adjacent mica surface and bind to both mica surfaces. Films of Tren(KGG-Cat)3 also show the largest increases in pull-off force ($F_{t=60 \text{ min}}/F_{t=10 \text{ s}} > 1$) and decreases in film thickness (ΔD_t), consistent with increased mobility of catechol functionalities. Alternatively, because the lysine residues of Tren(KGG-Cat)3 are close to the cationic Tren core, positive charge is localized at the center of the molecule. This localized charge density may enhance intermolecular cation-pi interactions and strengthen cohesion between symmetric monolayers, consistent with recent studies demonstrating the importance of cation-pi interactions in the adhesion and cohesion of materials containing catechol and cationic functionalities.35,36 Under this interpretation, the low pull-off force mediated by Tren(GGK-Cat)₃ at $D_t = 30 \text{ Å}$ suggests that the monolayers become sufficiently densely packed to bury the charged groups and inhibit cation-pi interactions between adjacent films.

To confirm that catechol-cation synergy was occurring, we measured forces mediated by siderophore analogs with cationic amines but without catechols (Tren(GGK-Benz)3, Figure 1G) and forces mediated by analogs with only catechol functionalities (Tren(GGG-Cat)3, Figure 1H), with representative force-distance plots shown in Figures S34 and S36. Consistent with previous studies,^{27,28} these molecules mediated much lower pull-off forces than siderophore analogs containing catechol and cationic amine functionalities. Films of Tren(GGK-Benz)₃ showed a >50% decrease in pulloff forces relative to Tren(GGK-Cat)₃ (Figure S33). The pulloff force likely results from adhesive electrostatic interactions between pendant cationic amines and the mica surfaces and cohesive hydrophobic and cation-pi interactions. Films of Tren(GGK-Benz)₃ also exhibited long-range repulsion on compression that decreased over sequential compression and separation cycles, indicating rearrangement of adsorbed aggregates. Properties of films of Tren(GGK-Benz)3 are described in Figure S35. Tren(GGG-Cat)3 showed no evidence of adsorption in the SFA after a 5-hour incubation, with onset of interaction, compressed film thickness, and pull-off force remaining identical to the values measured for bare mica surfaces in salt solution. Over 144 h, pulloff force progressively decreased from ~3 mN/m (micamica adhesion in salt solution) to zero as the compressed film thickness increased from <1 nm to 50 nm. These changes indicate the adsorption of multilayer aggregates on the mica surfaces, likely driven by electrostatic attraction between the cationic Tren scaffold and the negatively charged mica. The presence of adsorbed aggregates after 24- and 48-hour incubations of Tren(GGG-Cat)3 on mica was

confirmed with AFM (Figure S43). Pull-off force mediated by the aggregates depends on the separation velocity (Figure S36), suggesting that the aggregates are weakly associated and that the pull-off force results from energy dissipation. The delayed adsorption of Tren(GGG-Cat)₃ (over hours rather than minutes) suggests that cationic amines of the lysine residues drive adsorption onto the mica surface. Therefore, hydrogen bonds (involving the catechol functionalities or the peptide backbones of each arm of the siderophore analogs), electrostatic interactions involving the Tren core, and non-specific van der Waals interactions are insufficient to drive rapid adsorption of siderophore analogs into monolayers on the mica.

Above, we demonstrate the two criteria necessary for confirming the presence of catechol-cation synergy. We identify pull-off forces corresponding to a monolayer of siderophore analogs, therefore guaranteeing adhesive failure. We then show that siderophore analogs with catechol and cationic amine functionalities mediate significantly larger adhesion than analogs with either catechols or cationic amines alone. Importantly, the molecular weight and density of catechol and cationic amine functionalities were the same for Tren(GGK-Cat)₃, Tren(GKG-Cat)₃, and Tren(KGG-Cat)3. Since molecular weight37 and density of binding functionalities²⁸ influence the adsorption and adhesion of small molecules, keeping these quantities constant enables direct comparison of the adhesion forces to assess the impact of intramolecular spacing on catechol-cation synergy. Surprisingly, increasing the intramolecular catechol-cation spacing by up to two glycine residues does not catechol-cation synergy—Tren(GGK-Cat)3, abolish Tren(GKG-Cat)₃, and Tren(KGG-Cat)₃ all mediate the same maximum pull-off force (Figure S33). Therefore, direct intramolecular proximity is not necessary for catechol-cation synergy.

To further explore the impact of catechol-cation spacing on adhesion, we synthesized siderophore analogs with three and six glycine residues separating 2,3-DHBA and lysine, Tren(KGGG-Cat)3 and Tren(KGGGGGG-Cat)3, respectively. As expected, both molecules mediate substantial pull-off forces despite the increased catechol-cation spacing (Figures S38 and S40). However, the pull-off forces were lower than the pull-off forces for Tren(GGK-Cat)3, Tren(GKG-Cat)3, and Tren(KGG-Cat)3. Figure 7 shows a plot of pull-off force vs. molecular weight for various siderophore analogs containing catechol and cationic amine functionalities. The adhesion of Tren(K-Cat)3 reported in a previous study²⁷ remains the highest of all the siderophore analogs studied thus far due to its relatively low molecular weight and correspondingly large catechol-cation density. As molecular weight increases, pull-off force monotonically decreases, which we attribute to the decreasing density of catechol functionalities within each molecule. The gradually decreasing pull-off force due to decreasing binding group density is fundamentally different from an abrupt decrease in pull-off force at some intramolecular cut-off distance that abolishes catechol-cation synergy. Since adhesion force decreases gradually with catechol-cation spacing up to a spacing of six glycine residues, our results suggest that no such cut-off distance exists, and that further increases in

catechol-cation spacing will continue to gradually decrease the adhesion force even as catechol-cation synergy persists.

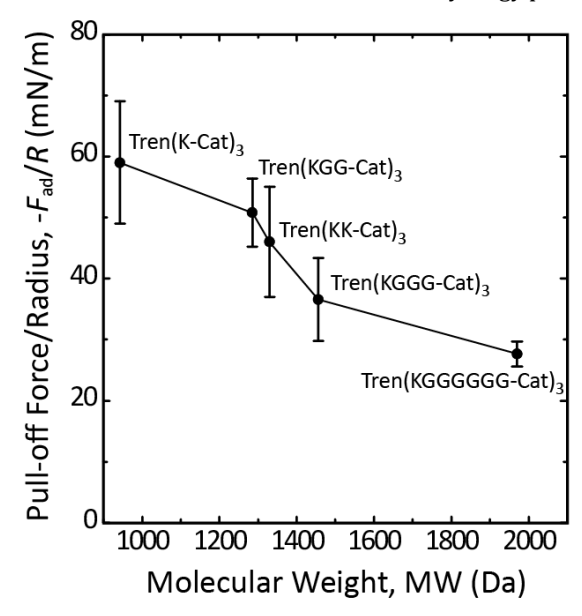


Figure 7. Plot of pull-off force $(-F_{\rm ad}/R)$ for $t_{\rm wait}=10$ s vs. molecular weight (MW) for siderophore analogs containing catechol and cationic amine functionalities. Data for Tren(K-Cat)₃ ($t_{\rm wait}=2$ min) and Tren(KK-Cat)₃ ($t_{\rm wait}=10$ min) reproduced from references (27) and (28), respectively. Lines included to guide the eye.

The results also suggest that the simultaneous detachment of catechol and cationic functionalities from the surface does not contribute to catechol-cation synergy in our experiments. Detachment order has been proposed to contribute to catechol-cation synergy in single-molecule adhesion studies, where the pulling geometry is precisely determined.29 Unlike single-molecule studies, our experiments involve ~108 siderophore analog molecules binding to mica (assuming each analog occupies 1 nm² on the mica surface) and a distribution of binding geometries. For example, the adjacent glycine residues in the peptide arms of Tren(KGG-Cat)3 are expected to give conformational flexibility to the molecule34 and consequently enable a range of distances between surface-bound catechol and cationic amine functionalities in a single siderophore analog arm. For the case where the catechol and cationic amine bind to the mica surface in close proximity (<1 nm), the cationic amine is expected to detach first during adhesive failure due to geometric considerations. For the case where the catechol and cationic amine bind relatively far apart on the mica (~2 nm), simultaneous detachment is possible. However, such distant binding is unlikely for entropic reasons, and therefore sequential catechol-cation detachment from the mica is expected to occur for the majority of Tren(KGG-Cat)₃ molecules in the contact area. In contrast, simultaneous detachment of catechol and cationic functionalities from the mica surface is more likely for Tren(GGK-Cat)₃ due to the intramolecular adjacency of those functionalities. If detachment order were necessary for catechol-cation synergy in our experiments, Tren(GGK-Cat)3 would be expected to mediate larger adhesion forces than Tren(KGG-Cat)3. Since Tren(GGK-Cat)₃, Tren(GKG-Cat)₃, and Tren(KGG-Cat)₃ mediate the same adhesion forces, we conclude that detachment order of catechol and cationic amine functionalities does not contribute to catechol-cation synergy in this work.

Based on our results, we propose the following mechanism for catechol-cation adhesion synergy: pendant cationic amines of the siderophore analogs exchange with adsorbed cations on the mica surface and drive adsorption onto the mica, enabling subsequent binding of catechols to the mica. With a monolayer of siderophore analogs on the surface, the effective concentration of catechols within 1 nm of the surface is $\sim\!\!3$ M, much greater than the bulk siderophore analog concentration (90-667 μM). This effective catechol concentration is calculated assuming that siderophore analogs bind to every negative charge on the mica lattice (1 e⁻ per 0.5 nm²). We suggest that the increased concentration of catechols near the mica surface increases the probability of catechols replacing surface-bound cations and binding to the mica.

To justify our mechanism for catechol-cation synergy we developed a qualitative model based on Bell Theory³⁸ to predict the lifetime and fractional surface coverage of cationic species adsorbed on the mica surface, further described in the Supporting Information (S5). The model predicts that siderophore analogs can adsorb to mica solely via their cationic amines. While the assumptions made in the derivation of the model preclude quantitative comparison with experiments, the predictions are qualitatively consistent with our experimental results showing that siderophore analogs lacking cationic functionalities do not adsorb into adhesive monolayers on mica in an aqueous electrolyte solution. As such, the role of cations in catechol-cation synergy is to drive adsorption onto negatively charged surfaces and enable subsequent binding of catechol functionalities. The cooperative effect operates irrespective of the intramolecular catechol-cation spacing. This result is surprising given that the majority of catechols in the most adhesive interfacial mussel protein are located directly adjacent to cationic amines and raises a fundamental biological question about the evolutionary pressure(s) responsible for this residue distribution.

4. CONCLUSIONS

This work explores the effect of intramolecular separation of catechol and cationic functionalities on adhesion mediated by monolayers of siderophore analog surface primers. Our results demonstrate that the pull-off force required to separate mica surfaces depends critically on the siderophore analog adsorption density, highlighting the importance of failure mode on adhesive performance. Furthermore, direct intramolecular adjacency of catechol and cationic amine functionalities is not necessary for catechol-cation synergy. Instead, increasing the intramolecular catechol-cation spacing in an adhesive by the addition of nonbinding domains progressively reduces adhesion due to the reduced density of binding groups. In sum, the results presented here explain the synergistic binding of catechol and cationic functionalities and should guide the design of new adhesives for binding to negatively charged surfaces in saline environments.

ASSOCIATED CONTENT

Supporting Information.

Details on the synthesis and characterization of siderophore analogs and the experimental methods using a surface forces apparatus (SFA) and atomic force microscope (AFM). This material is available free of charge via the Internet at http://pubs.acs.org.

AUTHOR INFORMATION

Corresponding Author

*butler@chem.ucsb.edu

Author Contributions

All authors have given approval to the final version of the manuscript.

ACKNOWLEDGMENTS

The authors thank J. Herbert Waite for his insightful comments. GDD was supported by the National Science Foundation Graduate Research Fellowship Program under Grant No. 1650114. AB is grateful for support from NSF CHE-1710761. The research reported here made use of shared facilities of the UCSB MRSEC (NSF DMR 1720256), a member of the Materials Research Facilities Network (www.mrfn.org).

REFERENCES

- (1) Danner, E. W.; Kan, Y.; Hammer, M. U.; Israelachvili, J. N.; Waite, J. H. Adhesion of Mussel Foot Protein Mefp-5 to Mica: An Underwater Superglue. *Biochemistry* **2012**, *51* (33), 6511–6518.
- (2) Lu, Q.; Danner, E.; Waite, J. H.; Israelachvili, J. N.; Zeng, H.; Hwang, D. S. Adhesion of Mussel Foot Proteins to Different Substrate Surfaces. J. R. Soc. Interface 2012, 10 (79), 20120759–20120759.
- (3) Yu, J.; Kan, Y.; Rapp, M.; Danner, E.; Wei, W.; Das, S.; Miller, D. R.; Chen, Y.; Waite, J. H.; Israelachvili, J. N. Adaptive Hydrophobic and Hydrophilic Interactions of Mussel Foot Proteins with Organic Thin Films. *Proc. Natl. Acad. Sci. U. S. A.* 2013, 110 (39), 15680–15685.
- (4) Waite, J. H. Mussel Adhesion Essential Footwork. J. Exp. Biol. 2017, 220 (4), 517–530.
- (5) Waite, J. H.; Qin, X. Polyphosphoprotein from the Adhesive Pads of Mytilus Edulis. *Biochemistry* **2001**, 40 (9), 2887–2893.
- (6) Lee, H.; Dellatore, S. M.; Miller, W. M.; Messersmith, P. B. Mussel-Inspired Surface Chemistry for Multifunctional Coatings. Science 2007, 318.
- (7) Hong, S.; Na, Y. S.; Choi, S.; Song, I. T.; Kim, W. Y.; Lee, H. Non-Covalent Self-Assembly and Covalent Polymerization Co-Contribute to Polydopamine Formation. Adv. Funct. Mater. 2012, 22 (22), 4711– 4717
- (8) Liebscher, J.; Mrówczyński, R.; Scheidt, H. A.; Filip, C.; Haìdade, N. D.; Turcu, R.; Bende, A.; Beck, S. Structure of Polydopamine: A Never-Ending Story? *Langmuir* 2013, 29 (33), 10539–10548.
- (9) Delparastan, P.; Malollari, K. G.; Lee, H.; Messersmith, P. B. Direct Evidence for the Polymeric Nature of Polydopamine. Angew. Chemie - Int. Ed. 2019, 58 (4), 1077–1082.
- (10) Ryu, J. H.; Messersmith, P. B.; Lee, H. Polydopamine Surface Chemistry: A Decade of Discovery. ACS Appl.

- Mater. Interfaces 2018, 10 (9), 7523-7540.
- (11) Kim, K.; Kim, K.; Ryu, J. H.; Lee, H. Chitosan-Catechol: A Polymer with Long-Lasting Mucoadhesive Properties. *Biomaterials* **2015**, *52* (1), 161–170.
- (12) Shin, M.; Park, S. G.; Oh, B. C.; Kim, K.; Jo, S.; Lee, M. S.; Oh, S. S.; Hong, S. H.; Shin, E. C.; Kim, K. S.; Kang, S. W.; Lee, H. Complete Prevention of Blood Loss with Self-Sealing Haemostatic Needles. *Nat. Mater.* 2017, 16 (1), 147–152.
- (13) Ryu, J. H.; Hong, S.; Lee, H. Bio-Inspired Adhesive Catechol-Conjugated Chitosan for Biomedical Applications: A Mini Review. *Acta Biomater.* **2015**, *27*, 101–115.
- (14) Lee, H.; Park, T. G.; Messersmith, P. B.; Lee, Y.; Statz, A. R.; Rho, J. Substrate-Independent Layer-by-Layer Assembly by Using Mussel-Adhesive-Inspired Polymers. *Adv. Mater.* **2008**, *20* (9), 1619–1623.
- (15) Kim, E.; Song, I. T.; Lee, S.; Kim, J. S.; Lee, H.; Jang, J. H. Drawing Sticky Adeno-Associated Viruses on Surfaces for Spatially Patterned Gene Expression. *Angew. Chemie Int. Ed.* 2012, 51 (23), 5598–5601.
- (16) Statz, A. R.; Meagher, R. J.; Barron, A. E.; Messersmith, P. B. New Peptidomimetic Polymers for Antifouling Surfaces. J. Am. Chem. Soc. 2005, 127 (22), 7972–7973.
- (17) Ahn, B. K.; Das, S.; Linstadt, R.; Kaufman, Y.; Martinez-Rodriguez, N. R.; Mirshafian, R.; Kesselman, E.; Talmon, Y.; Lipshutz, B. H.; Israelachvili, J. N.; et al. High-Performance Mussel-Inspired Adhesives of Reduced Complexity. *Nat. Commun.* 2015, 6, 8663.
- (18) Chirdon, W. M.; O'Brien, W. J.; Robertson, R. E. Adsorption of Catechol and Comparative Solutes on Hydroxyapatite. *J. Biomed. Mater. Res. Part B Appl. Biomater.* **2003**, *66* (2), 532–538.
- (19) Li, Y.; Qin, M.; Li, Y.; Cao, Y.; Wang, W. Single Molecule Evidence for the Adaptive Binding of DOPA to Different Wet Surfaces. *Langmuir* **2014**, *30* (15), 4358–4366.
- (20) Lee, B. P.; Messersmith, P. B.; Israelachvili, J. N.; Waite, J. H. Mussel-Inspired Adhesives and Coatings. *Annu. Rev. Mater. Res.* 2011, 41 (1), 99–132.
- (21) Fortelny, R. H.; Petter-Puchner, A. H.; Walder, N.; Mittermayr, R.; Öhlinger, W.; Heinze, A.; Redl, H. Cyanoacrylate Tissue Sealant Impairs Tissue Integration of Macroporous Mesh in Experimental Hernia Repair. Surg. Endosc. Other Interv. Tech. 2007, 21 (10), 1781–1785.
- (22) Kocherov, S.; Lev, G.; Chertin, B. Use of BioGlue Surgical Adhesive in Hypospadias Repair. *Curr. Urol.* **2014**, *7* (3), 132–135.
- (23) Montanaro, L.; Arciola, C. .; Cenni, E.; Ciapetti, G.; Savioli, F.; Filippini, F.; Barsanti, L. . Cytotoxicity, Blood Compatibility and Antimicrobial Activity of Two Cyanoacrylate Glues for Surgical Use. *Biomaterials* **2000**, *22* (1), 59–66.
- (24) Fürst, W.; Banerjee, A. Release of Glutaraldehyde from an Albumin-Glutaraldehyde Tissue Adhesive Causes Significant in Vitro and in Vivo Toxicity. *Ann. Thorac. Surg.* **2005**, *79* (5), 1522–1528.

- (25) Klimo, P.; Khalil, A.; Slotkin, J. R.; Smith, E. R.; Scott, R. M.; Goumnerova, L. C. Wound Complications Associated with the Use of Bovine Serum Albumin-Glutaraldehyde Surgical Adhesive in Pediatric Patients. *Neurosurgery* 2007, 60 (4 SUPPL. 2), 305–309.
- (26) Saiz-Poseu, J.; Mancebo-Aracil, J.; Nador, F.; Busqué, F.; Ruiz-Molina, D. The Chemistry behind Catechol-Based Adhesion. Angew. Chemie - Int. Ed. 2019, 58 (3), 696– 714.
- (27) Maier, G. P.; Rapp, M. V; Waite, J. H.; Israelachvili, J. N.; Butler, A. Adaptive Synergy between Catechol and Lysine Promotes Wet Adhesion by Surface Salt Displacement. *Science* 2015, 349 (6248), 625–628.
- (28) Rapp, M. V; Maier, G. P.; Dobbs, H. A.; Higdon, N. J.; Waite, J. H.; Butler, A.; Israelachvili, J. N. Defining the Catechol-Cation Synergy for Enhanced Wet Adhesion to Mineral Surfaces. J. Am. Chem. Soc. 2016, 138 (29), 9013–9016.
- (29) Li, Y.; Wang, T.; Xia, L.; Wang, L.; Qin, M.; Li, Y.; Wang, W.; Cao, Y. Single Molecule Study of the Synergistic Effects of Positive Charges and Dopa for Wet Adhesion. J. Mater. Chem. B 2017.
- (30) Sandy, M.; Butler, A. Chrysobactin Siderophores Produced by Dickeya Chrysanthemi Ec16. *J. Nat. Prod.* **2011**, *74* (5), 1207–1212.
- (31) Israelachvili, J.; Min, Y.; Akbulut, M.; Alig, A.; Carver, G.; Greene, W.; Kristiansen, K.; Meyer, E.; Pesika, N.; Rosenberg, K.; Zeng, H. Recent Advances in the Surface Forces Apparatus (SFA) Technique. *Reports Prog. Phys.* 2010, 73 (3), 036601.
- (32) Paria, S.; Khilar, K. C. A Review on Experimental Studies of Surfactant Adsorption at the Hydrophilic Solid-Water Interface. *Adv. Colloid Interface Sci.* **2004**, *110* (3), 75–95.
- (33) Halperin, A. Polymer Brushes That Resist Adsorption of Model Proteins: Design Parameters. *Langmuir* **1999**, *15* (7), 2525–2533.
- (34) Ramachandran, G. N.; Ramakrishnan, C.; Sasisekharan, V. Stereochemistry of Polypeptide Chain Configurations. J. Mol. Biol. 1963, 7 (1), 95–99.
- (35) Gebbie, M. A.; Wei, W.; Schrader, A. M.; Cristiani, T. R.; Dobbs, H. A.; Idso, M.; Chmelka, B. F.; Waite, J. H.; Israelachvili, J. N. Tuning Underwater Adhesion with Cation–π Interactions. *Nat. Chem.* **2017**, *9*, 473–479.
- (36) Hong, S.; Wang, Y.; Park, S. Y.; Lee, H. Progressive Fuzzy Cation- Assembly of Biological Catecholamines. Sci. Adv. 2018, 4 (9), eaat7457.
- (37) Wei, W.; Yu, J.; Gebbie, M. A.; Tan, Y.; Martinez Rodriguez, N. R.; Israelachvili, J. N.; Waite, J. H. Bridging Adhesion of Mussel-Inspired Peptides: Role of Charge, Chain Length, and Surface Type. *Langmuir* **2015**, *31* (3), 1105–1112.
- (38) Bell, G. I. Models for the Specific Adhesion of Cells to Cells. *Science* **1978**, *200*, 618–627.

Insert Table of Contents artwork here

